

Irradiation effects in Ag-Fe bilayers: Ion-beam mixing, recrystallization, and surface roughening

Alejandro Crespo-Sosa, Peter Schaaf, Wolfgang Bolse, and Klaus-Peter Lieb

II. Physikalisches Institut and Sonderforschungsbereich 345, Universität Göttingen, Bunsenstr. 7/9, D-37073 Göttingen, Germany

Matthias Gimbel and Ulrich Geyer

I. Physikalisches Institut and Sonderforschungsbereich 345, Universität Göttingen, Bunsenstr. 9, D-37073 Göttingen, Germany

Cristiana Tosello

Universita di Trento, Dipartimento di Fisica, Via Sommarive, I-38050 Trento, Italy

(Received 15 September 1995; revised manuscript received 11 December 1995)

Ag/Fe bilayers deposited onto SiO₂/Si substrates were irradiated at 20, 77, and 300 K with 300–750 keV Ar and Xe ions in order to study the ion-beam-induced mixing and phase formation in this thermally immiscible system. A combination of Rutherford backscattering spectroscopy (RBS), channeling, conversion electron Mössbauer spectroscopy (CEMS), and scanning tunneling microscopy (STM) was used to analyze the atomic transport at the interface and the resulting microstructure and morphology changes of the samples. In the CEMS measurements, a 13 nm thin ⁵⁷Fe marker layer at the Ag/Fe interface was introduced in order to enhance the sensitivity to alterations of the interfacial composition. From the small amount of Ag atoms found to be dissolved in Fe and from the sharpness of the element profiles at the interface, we derived a very small mixing efficiency, which is significantly smaller than the prediction of the ballistic model. Since ballistic mixing is expected in any case, we argue that demixing and phase separation occur in the relaxation stage or thermal spike phase of the collision cascade, as a consequence of the positive heat of mixing. On the other hand, ion irradiation induces a large surface roughening of the Ag top layer as proven by STM. This effect is obviously due to recrystallization of Ag, which results in grain growth and texture formation along the direction of the impinging ion, as demonstrated by RBS/channeling measurements. [S0163-1829(96)02921-9]

I. INTRODUCTION

Since the beginning of the 1980's, ballistic mechanisms during ion-beam mixing have been recognized and described by Sigmund and Gras-Martí.^{1,2} According to their model, ion-beam mixing only depends on the kinematic properties of the materials, it always takes place, and it is independent of the chemical properties of the system. The most important parameter is the energy density, F_D , deposited at the interface in primary and secondary elastic collisions.

Transient diffusion in thermal spikes was proposed when it became evident that in most bilayer systems the measured mixing rates were up to ten times larger than those predicted ballistically.³ Such diffusion processes can be biased by chemical driving forces and, indeed, an increasing amount of mixing was found for increasing chemical affinities in kinematically similar bilayer couples.⁴ The influence of the cohesive enthalpy (ΔH_{coh}) and the heat of mixing (ΔH_{mix}) in thermal spikes has been delineated in some models, giving rise to a Darken-type enhancement of the mixing process. Cheng,⁵ using fractal theory, determined that a mean atomic number (\bar{Z}) larger than 20 was a necessary condition for the formation of thermal spikes. In most of the cases, the consideration of the chemical driving forces within these models accounts for the difference between the ballistic mixing rates and the experimental data. The experimental observation⁶ presented in Fig. 1 is also reproduced by these models: the higher the chemical affinity ($\Delta H_{\text{mix}}/\Delta H_{\text{coh}}$), the larger the ion-beam mixing. In this figure, ion-beam mixing is expressed by the reduced mixing efficiency η_{red} :

$$\eta_{\text{red}} = 2k \frac{N^{2/3} (\Delta H_{\text{coh}})^2}{\bar{Z}^{1.77} F_D}, \quad (1)$$

where N is the mean atomic density of the target material and k is the mixing rate $\Delta\sigma^2/\Phi$. Nevertheless, in all these models the chemical driving forces have been assumed to be favorable for mixing in systems with negative heat of mixing.

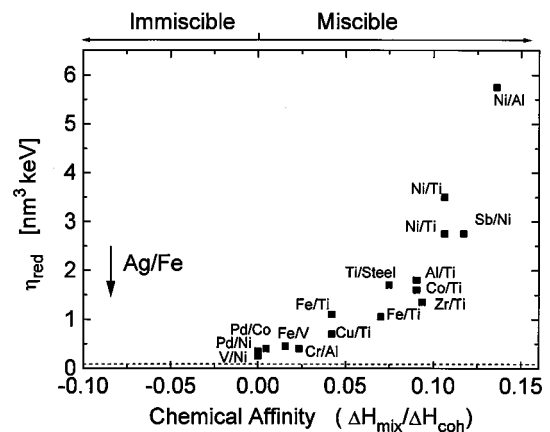


FIG. 1. Reduced mixing efficiency η_{red} observed for various bilayer couples as a function of the chemical affinity of top and bottom layers. The data were taken from Ref. 6. The prediction of the ballistic model is represented by the horizontal dashed line, the arrow indicates the position of the Ag/Fe system.

TABLE I. Geometry of the samples used in this work: ion, ion energy, irradiation temperature, substrate, Fe thickness d_{Fe} , initial Ag thickness d_{Ag}^i , final Ag thickness d_{Ag}^f , maximum ion fluence Φ^{max} , projected range R_p and range straggling ΔR_p .

Ion & Energy	Temp. (K)	Substrate	d_{Fe} (nm)	d_{Ag}^i (nm)	d_{Ag}^f (nm)	Φ^{max} (10^{15} ions/cm ²)	R_p^a (nm)	ΔR_p^a (nm)
Ar 300 keV	20	Si	95	90	67	60	120	48
	77 ^b	Si	150	110	80	60	120	48
	77 ^c	Si	150	105	53	70	120	48
	300	Si	150	105	53	60	120	48
Xe 750 keV	20	Si	95	70	58	10	97	36
	77 ^b	Si	150	70	50	8	97	36
	77 ^c	Si	150	65	48	7	97	36
450 keV	300	Si	150	95	75	8	95	31
	77	SiO ₂	70 ^d	50	26	8	61	25

^aCalculated with TRIM, version 1992.

^bSingle step irradiation.

^cSequential irradiation.

^dWith a 13 nm ⁵⁷Fe marker layer.

Until some years ago,⁷ little theoretical and experimental work had been done, in systems with positive heats of mixing (i.e., thermally immiscible systems) like Cu/Bi, Cu/Nb, and Cu/Mo,⁸ Fe/Cu,⁹ Fe/Mg,¹⁰ and Ag/Ni,^{11,12} but now they are of growing interest as their usefulness in understanding the basic ion-beam-mixing processes has been recognized. For this reason, the system silver-iron with its large positive heat of mixing ($\Delta H_{\text{mix}} = +42$ kJ/mole at equiatomic composition, or even in the liquid state $\Delta H_{\text{mix}}^{\text{liq}} = +28$ kJ/mole),¹³ and its mean atomic number ($\bar{Z} = 36.5$, favoring, according to Cheng's analysis,⁵ the formation of thermal spikes) is of particular interest. In addition, the difference in mass permits the analysis with Rutherford backscattering spectroscopy (RBS) and the ⁵⁷Fe isotope can be used to study the microstructure via Mössbauer spectroscopy.

II. EXPERIMENTAL

A. Sample preparation

The bilayer samples were prepared by subsequent deposition of Fe and Ag films on water-cooled silicon (100) substrates by electron gun evaporation. The iron films of 70–150 nm thickness were deposited at a typical rate of 0.2–0.3 nm/s, as monitored by a quartz oscillator, and at a pressure lower than 10^{-4} Pa during evaporation. Fe films thicker than 150 nm could not be prepared because of delamination due to intrinsic stresses. Subsequently, without breaking the vacuum and under the same conditions, 60–110 nm thick silver films were deposited onto the Fe layer. The thicknesses of the Ag films were chosen depending on the ion species and energies they were to be irradiated with. In this way, the desired deposited energy density at the interface (F_D) could be adjusted and the complicating effects of surface sputtering could be decoupled as much as possible from the processes taking place at the interface.

Bilayers of Ag/Fe with a 13 nm marker of (95% isotopically enriched) ⁵⁷Fe at the interface were deposited onto SiO₂/Si substrates by successive evaporation of the three components under ultrahigh vacuum (UHV) conditions. The

base pressure in the evaporation chamber was 6×10^{-6} Pa and about 1×10^{-5} Pa during film deposition. The evaporation was performed by means of an electron gun for Fe and Ag and by a W crucible heated by the Joule effect for ⁵⁷Fe. The deposition rate for all the elements was kept at 1.2–1.8 nm/min and controlled by means of a quartz oscillator. The thicknesses of the layers were 50(± 1) nm Ag, 13 (± 1.2) nm ⁵⁷Fe and 54(± 1.5) nm Fe on 150 nm SiO₂/Si substrates. The substrates were kept at 300 K during evaporation. The detailed geometries of the samples are listed in Table I.

B. Ion implantation

Ion implantation at 300, 77, and in two cases at 20 K was performed at the Göttingen 530 kV implanter IONAS.¹⁴ The ion species used were Ar⁺, Xe⁺, and Xe⁺⁺ with energies ranging between 300 and 750 keV. The corresponding projected ion ranges as calculated with the TRIM code (version 1992)¹⁵ are listed in Table I. Typical beam currents measured at the target were about 1–4 μA over a 1×1 cm² surface area. Homogeneous implantation was achieved by means of an electrostatic X-Y sweeping system. The effects of irradiation as a function of the ion fluence Φ were investigated in two different ways: (a) a single sample was irradiated in sequential steps and analyzed after each irradiation with the different methods (sequential irradiation) or (b) different identically prepared samples were irradiated at the desired ion fluence in a single step (single step irradiation).

The energy density F_D deposited at the interface via elastic collisions was determined by means of the TRIM (Ref. 15) code, taking into account the higher generation recoils. F_D is actually smaller than the nuclear stopping power (S_n) of the ion, since the recoil atoms themselves lose their kinetic energy by both elastic nuclear and inelastic electronic stopping. Furthermore, the spatial distribution of F_D might differ from that of S_n because of the energy transport by the primary recoils. The deposited energy F_D is related to the number of relocated atoms by⁶

$$F_D = (2n_D + n_R)E_D, \quad (2)$$

where n_D and n_R denote the number of displacement and replacement collisions per unit path length and E_D is the displacement threshold (≈ 20 eV). Because of sputtering, the Ag film gets thinner as it is bombarded, i.e., its thickness $d(\Phi)$ is a function of the ion fluence Φ . From the TRIM (Ref. 15) simulations it has been found that the energy deposited at the interface depends on the top layer thickness and thus varies with the ion fluence Φ . Therefore, an average deposited energy density is considered:

$$\bar{F}_D = \frac{1}{\Phi_{\max}} \int_0^{\Phi_{\max}} F_D(d(\Phi)) d\Phi. \quad (3)$$

As confirmed by the experimental observations, $d(\Phi) = d_o - Y\Phi$ is a linear function of the ion fluence (where the slope Y corresponds to the sputtering rate) and a third-order polynomial can be fitted to $F_D(d)$ in order to perform the integral.

C. Rutherford backscattering spectroscopy

After deposition and after each irradiation step, the samples were analyzed by means of Rutherford backscattering spectroscopy (RBS), using the 900 keV He⁺⁺ beam of the Göttingen 530 kV implanter IONAS.¹⁴ The energy spectrum of the backscattered He⁺⁺ ions was measured using a silicon surface barrier detector under an angle of 165° with respect to the normally incident beam. The detector resolution (measured at the silver surface of each sample) was about 12 keV (full width at half maximum). Typical values for the beam current were between 5 and 15 nA (150–500 nA/cm²).

Except for two cases, where ion implantation and RBS were performed at 20 K without warming up the sample in between, all the RBS measurements were done at 300 K. For some selected samples, the texture of the Ag top layer, due to ion-induced recrystallization, was monitored by means of the channeling effect. For this purpose, an angular RBS scan with a well collimated He⁺⁺ beam was performed across the incidence angle of the implantation beam.

The spectra analysis was performed using the program RUMP.^{16,17} This program allows the simulation and fitting of an error-function-like composition profile of the elements involved:

$$C(x) = C_0 \left[1 - \frac{1}{2\sqrt{\pi}} \int_0^{(x-d)/\sqrt{2}\sigma_{\text{RBS}}} \exp(-z^2) dz \right], \quad (4)$$

where d is the interface position (top layer thickness) and σ_{RBS} is its standard deviation.

A typical RBS spectrum of a sample before and after irradiation with 750 keV Xe ions is shown in Fig. 2. The respective experimental depth distributions of Ag and Fe are plotted in Fig. 3, together with the fitted error function profiles. As observed in many other ion mixing experiments, the edges at the interface are less steep after irradiation, i.e., σ_{RBS}^2 increases with increasing ion fluence. However, one should note that σ_{RBS}^2 is composed of the variance of the

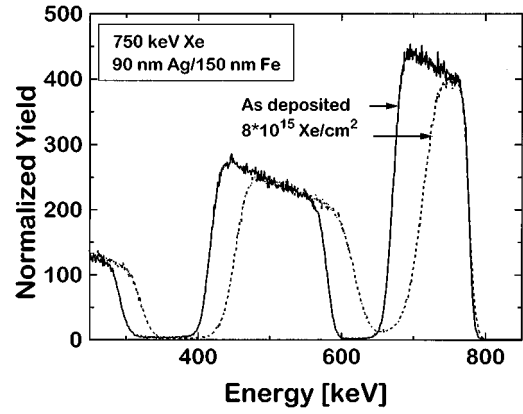


FIG. 2. RBS spectra of an Ag/Fe bilayer, as-deposited (solid line) and after irradiation with 8×10^{15} Xe/cm² of 750 keV at 77 K (dashed line).

interfacial concentration gradient, σ_{mix}^2 , and the lateral fluctuation of the top layer thickness, σ_d^2 , which itself contains both the interface and the surface roughness. In the present case, as will be demonstrated below, σ_d^2 is, to a large extent, determined by irradiation-induced Ag grain growth and the corresponding surface roughness of the Ag top layer. The influence of the surface roughness on the RBS spectra is schematically illustrated in Fig. 4. In a first-order approximation, the total effect at the Ag/Fe interface is given by $\sigma_{\text{RBS}}^2 = \sigma_d^2 + \sigma_{\text{mix}}^2$. If no damage were produced at the Fe/Si interface, its variance would reflect σ_d^2 only, and could thus be used to estimate the influence of the surface roughness on the variance observed for the Ag/Fe interface. However, we cannot exclude that mixing also occurs at the Fe/Si interface: although most ions were stopped in the Fe film, elastic energy at the Fe/Si interface was deposited by recoiling Fe

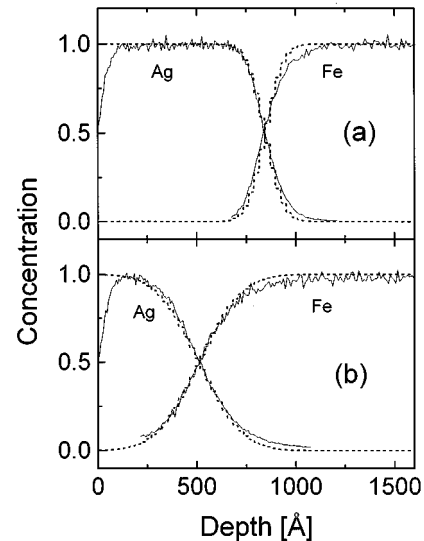


FIG. 3. Experimental concentration profiles obtained from the spectra shown in Fig. 2 (solid line). The dashed lines represent the fitted error function.

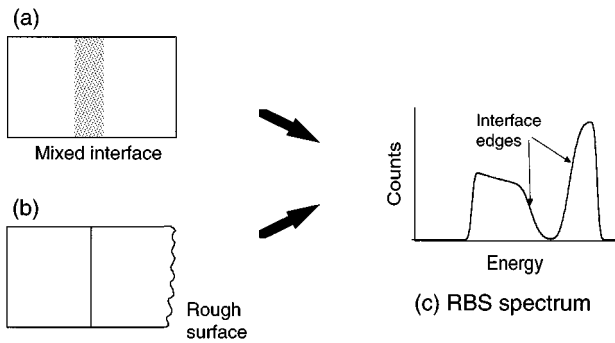


FIG. 4. Sketch of a bilayer with an intermixed interface (a), and of a bilayer with a rough surface (b). Both cases result in the same RBS spectrum (c).

atoms. In fact, the variance measured at the Fe/Si interface was generally larger than the one observed at that Ag/Fe interface.

D. Scanning tunneling microscopy

In order to quantify the surface roughness σ_d , scanning tunneling microscopy (STM) was performed. The measurements were done in air with a Nanoscope II microscope in constant current mode (0.05 – 1.1 nA). The bias voltage varied in the range 550–1000 mV, where no alterations of the surface during the STM measurements were observed. The scanning areas were 1000×1000 , 2000×2000 , and 4000×4000 nm². The variance of the height distribution of the STM scans

$$\sigma_{\text{STM}}^2 = \frac{1}{N-1} \sum_{i=1}^N (z_i - \bar{z})^2, \quad (5)$$

was taken as a measure of the surface roughness σ_d^2 . Here, N is the number of pixels (400×400) of the STM image, z_i the surface height at pixel i , and \bar{z} their average value. In order to achieve the most representative data, the height distribution obtained from the largest available scan was used. Here, it must be mentioned again that σ_d^2 might contain, in addition to the surface roughness, a contribution due to interface roughness. As will be justified below, there is no evidence for the presence of the latter in our data and we can consider σ_{STM}^2 as a measure of σ_d^2 . In most cases the height distribution (see Fig. 5) was Gaussian, however, there were also some non-Gaussian distributions. Although the variances of the data were always close (typically within 15%) to those of the Gaussian fits, in such cases σ_{RBS}^2 might not be a linear superposition any more of σ_{mix}^2 and σ_{STM}^2 .

E. Conversion electron Mössbauer spectroscopy

The samples having the ⁵⁷Fe enriched Ag/Fe interface were investigated with conversion electron Mössbauer spectroscopy (CEMS) in the as-deposited and the implanted state. All the spectra were taken at room temperature with a conventional He/6%CH₄-flow proportional counter¹⁸ and a constant acceleration drive with a ⁵⁷Co/Rh source (about 400 MBq). The spectra were analyzed by superimposing Lorentzian lines with a least-squares-fit program.¹⁹ Isomer shifts are always given relative to α -Fe at room temperature. It

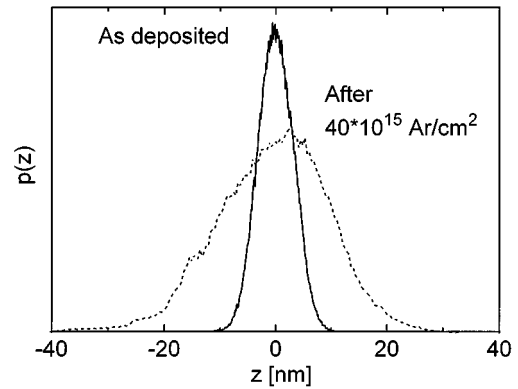


FIG. 5. Surface height distribution as measured with STM for a sample as-deposited (solid line, $\sigma_{\text{STM}} = 3.1(\pm 0.1)$ nm) and after irradiation at 77 K with 4×10^{16} Ar/cm² of 300 keV (dashed line, $\sigma_{\text{STM}} = 10.1(\pm 1.1)$ nm).

should be mentioned that, because of the energy loss of the conversion electrons, the information depth in Fe and Fe-based alloys is limited to about 100–150 nm.^{20,21} This is more than twice the depth of the ⁵⁷Fe layer in the samples reported here and hence more than 95% of the Mössbauer spectra originate from the ⁵⁷Fe-enriched layer.

III. RESULTS

A. RBS measurements

As mentioned above, RBS measures the depth distribution of the constituent materials of the Ag/Fe bilayers laterally averaged over the beam spot of 2 mm in diameter. As shown in Figs. 2 and 3, the irradiation results in a narrowing of the Ag top layer due to sputtering as well as a clear broadening of the interfacial edges of the Ag and Fe distribution. We again point out that this broadening, because of the lateral averaged signal, may be caused by atomic intermixing of the interface *and* roughening of the surface due to sputtering and/or recrystallization.

In Fig. 6(a), the related changes in the variances $\Delta \sigma_{\text{RBS}}^2 = \sigma_{\text{RBS}}^2(\Phi) - \sigma_{\text{RBS}}^2(0)$ are plotted as a function of the ion fluence Φ for the case of a sample sequentially irradiated at 77 K with 300 keV Ar⁺ ions. The nonlinear dependence should be noted, which is in contrast to the linear dependence usually reported for miscible systems and to the predictions of the theoretical models. The dispersion of the data points for individual samples irradiated at a different fluence each, as shown in Fig. 6(b), is too high to draw conclusions as to whether such deviation persists. The dispersion may be attributed to small differences in the preparation of the samples, which can lead to slightly different properties of the films and their surfaces. However, the broadening at high fluences seems to be smaller than in the case of sequentially irradiated samples. The broadening found after 20 K bombardment with Ar ions at $\Phi = 60 \times 10^{15}$ Ar/cm² is also displayed in Fig. 6 and it is only slightly smaller than those of the samples irradiated at 77 K. In the case of room-temperature single irradiations [Fig. 6(c)], the dispersion of the data is small and little deviation from linearity is observed. The samples irradiated with Xe ions, which are displayed in Fig. 7, present similar characteristics as discussed

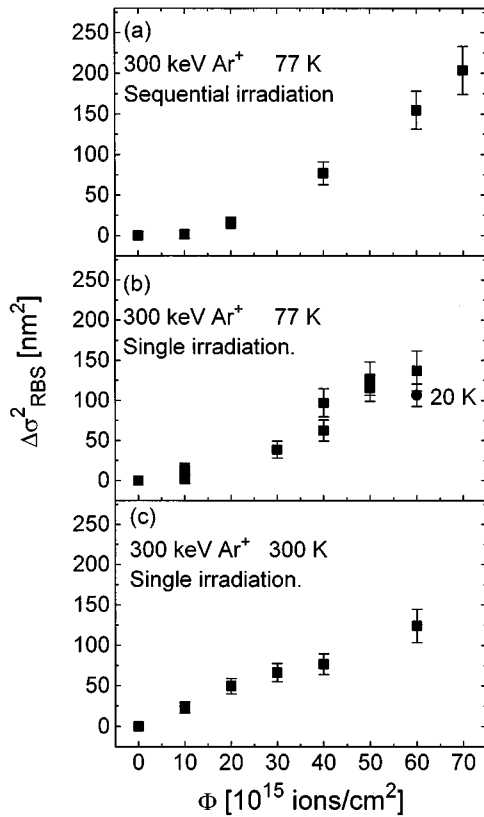


FIG. 6. Interface broadening $\Delta\sigma^2_{\text{RBS}}$ as a function of the ion fluence Φ measured with RBS: (a) for one single sample irradiated sequentially with 300 keV Ar at 77 K, (b) for a series of samples each of them irradiated in one single step with 300 keV Ar ions at 77 K and 20 K (circle), and (c) for a series of samples irradiated in one single step at 300 K with 300 keV Ar ions.

above. In Fig. 8, the RBS spectra of the sample irradiated with Ar ions at 20 K are shown. The spectra were taken at 20 K before and immediately after irradiation and also after warming up the sample to room temperature. An inspection of the high-energy edge of the Fe signal clearly shows that no additional broadening occurs during warming up of the sample. The Ag signal is affected by a channeling effect due to irradiation-induced recrystallization, as will be discussed below.

As indicated above, samples irradiated to high fluences in one step show a decrease in the RBS yield of the Ag top layer. Therefore, RBS-channeling scans were performed in order to test if this can be attributed to an irradiation-induced texture in the sample surface. For this purpose, specific samples were irradiated at 20, 77, and 300 K with Xe ions at normal incidence. In addition, one sample was irradiated at 77 K and an angle of about 15° with respect to the surface normal and another one at 20 K with normally incident Ar ions. Figure 9 shows the normalized Ag backscattering yield as a function of the tilt angle. A minimum value is found when the direction of the analyzing particles coincides with that of the implantation beam, indicating an increase in texture in the direction of the impinging ions. This effect is more pronounced for low-temperature irradiation. No channeling effect was observed for the as-deposited samples.

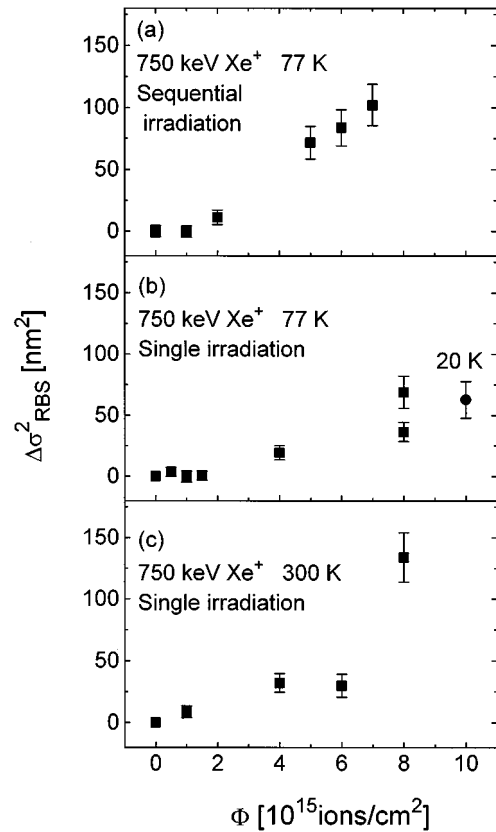


FIG. 7. Interface broadening $\Delta\sigma^2_{\text{RBS}}$ as a function of the ion fluence Φ measured with RBS: (a) for one single sample irradiated sequentially with 750 keV Xe at 77 K, (b) for a series of samples each of them irradiated in one single step with 750 keV Xe ions at 77 K and 20 K (circle), and (c) for a series of samples irradiated in one single step at 300 K with 750 keV Xe ions.

B. STM measurements

Selected samples were investigated by means of STM in order to examine the surface roughness before and after ion irradiation. In Fig. 10, the STM images of a virgin sample and of a sample irradiated with 300 keV Ar ions at 77 and at 300 K are displayed. The surface of the as-deposited sample

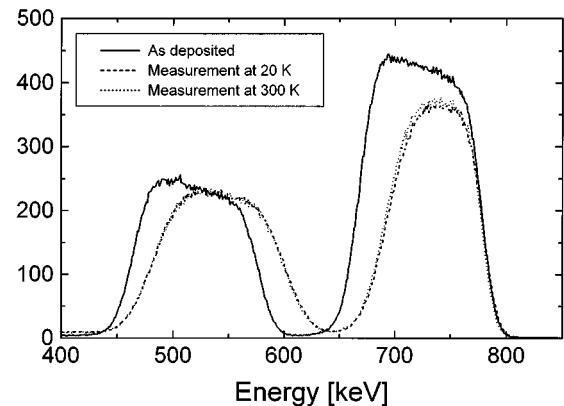


FIG. 8. Comparison of the spectra measured for a sample as-deposited (solid line), immediately after irradiation with $6 \times 10^{16} \text{ Ar/cm}^2$ at 20 K (dashed line) and after warming up the sample to room temperature (dotted line).

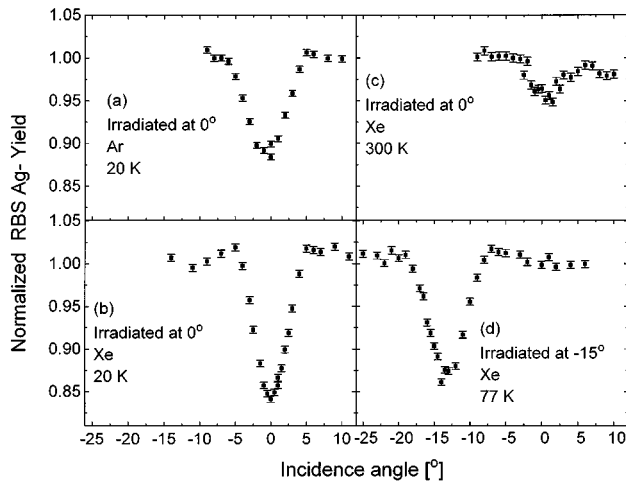


FIG. 9. Normalized RBS yield of the Ag film as a function of the tilt angle for samples irradiated under normal beam incidence with (a) 300 keV Ar ions at 20 K, (b) 750 keV Xe⁺⁺ ions at 300 K and (c) at 20 K, and (d) for a sample irradiated with Xe ions at 77 K and an incidence angle of 15°.

is flat and presents small grains. After room-temperature irradiation the grain size has increased remarkably and the surface has become much rougher. Such an increase in the grain size is also seen after 20 and 77 K irradiation, but here

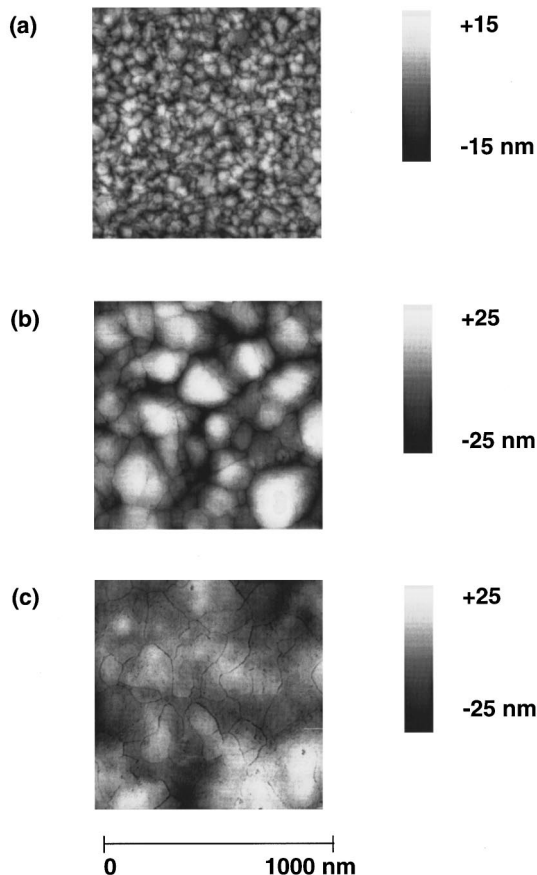


FIG. 10. STM images of (a) an as-deposited sample, (b) a sample irradiated with 4×10^{16} Ar/cm² at 300 K, and (c) a sample irradiated with 4×10^{16} Ar/cm² at 77 K.

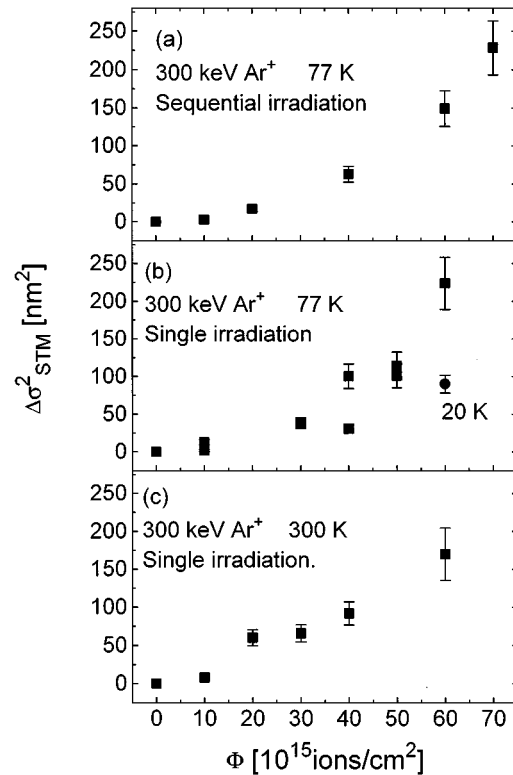


FIG. 11. Change of the roughness parameter, $\Delta\sigma_{\text{STM}}^2$, as a function of the ion fluence Φ measured with STM: (a) for one single sample irradiated sequentially with 300 keV Ar ions at 77 K, (b) for a series of samples each of them irradiated in one single step with Ar ions at 77 K, and (c) for a series of samples each of them irradiated in one single step at 300 K.

the surface consists of flat platelets, while in the case of the 300-K-irradiated sample spherically shaped grains are formed. No difference was observed between the images of the samples irradiated in one single step and those irradiated sequentially.

A quantitative analysis of the STM results is possible by evaluating the measured height distribution of the surface, as shown in Fig. 5. The second moment of the height distribution (σ_{STM}^2) increases with the ion fluence Φ , as shown in Fig. 11 for the cases of (a) one sample irradiated sequentially at 77 K, (b) a series of samples irradiated in one step at 77 K and (c) a series of samples irradiated in one step at 300 K. The value found after 20 K irradiation with 6×10^{16} Ar/cm² is also included in Fig. 11(b). Figure 12 shows the results for the samples irradiated with Xe ions. The curves present the same characteristics and magnitudes as in RBS, including the fact that the broadening observed at 20 K is slightly smaller than at 77 K.

C. Mössbauer measurements

A set of samples enriched in ⁵⁷Fe at the interface was studied with both RBS and Mössbauer spectroscopy. No other contribution, except that of pure α -Fe, was found in the Mössbauer spectra for any of the as-deposited samples. On the contrary, the spectra of the irradiated samples exhibit three additional magnetic subspectra^{22,23} which have been interpreted as follows: *M0* originates from Fe atoms with

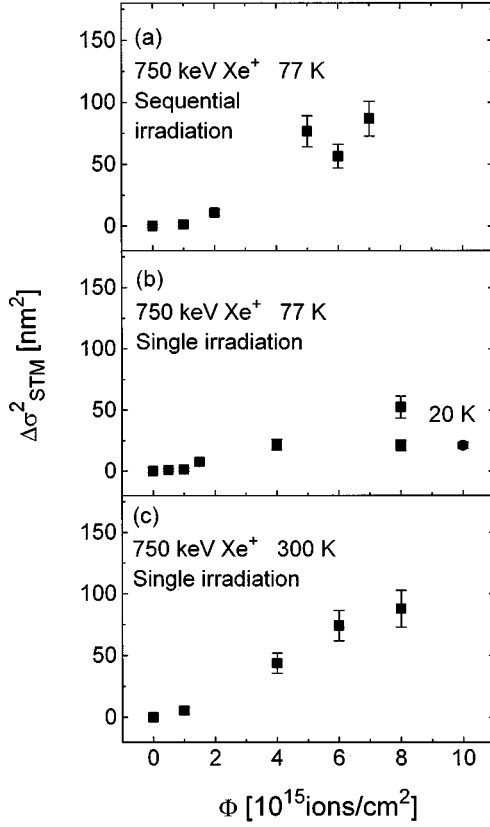


FIG. 12. Change of the roughness parameter, $\Delta\sigma_{STM}^2$, as a function of the ion fluence Φ measured with STM: (a) for one single sample irradiated sequentially with 750 keV Xe ions at 77 K, (b) for a series of samples each of them irradiated in one step with 750 keV Xe ions at 77 K and 20 K (circle), and (c) for a series of samples each of them irradiated in one step at 300 K with 750 keV Xe ions.

neighboring Ag atoms, but not as next neighbors, while $M1$ and $M2$ correspond to Fe atoms with one or two (or more) Ag atoms as next neighbors. As an example, the CEMS spectrum of a sample after a total fluence of 6×10^{15} Xe/cm² with 450 keV Xe⁺ ions at 77 K is shown in Fig. 13(a), while in Fig. 13(b) the α -Fe fraction in the spectra is given as a function of the ion fluence for samples irradiated at 77 and 300 K as well. This fraction decreases with increasing ion fluence and no significant difference can be observed between the two irradiation temperatures. The fractions of the other three magnetic subspectra, which correspond to Ag atoms dissolved in the Fe matrix, increase with increasing ion fluence as shown in Fig. 13(c). From the ratios between the fractions $M0$, $M1$, and $M2$, a 2.4 (± 0.3) at. % Ag concentration in α -Fe(Ag) can be calculated for the irradiation at 300 K considering a binomial distribution. At 77 K, this Ag concentration amounts to 2.8 (± 0.3) at. %.

Another sample that was also irradiated to a fluence of 6×10^{15} Xe/cm² with 450 keV Xe⁺ ions at 77 K, but in one single step, presented no significant difference in its Mössbauer results, in contrast to the difference in the broadening $\Delta\sigma_{RBS}^2$ observed with RBS for the two irradiation modes. This clearly shows that the latter is related to the changes at the surface and not at the interface, as seen by the STM analysis.

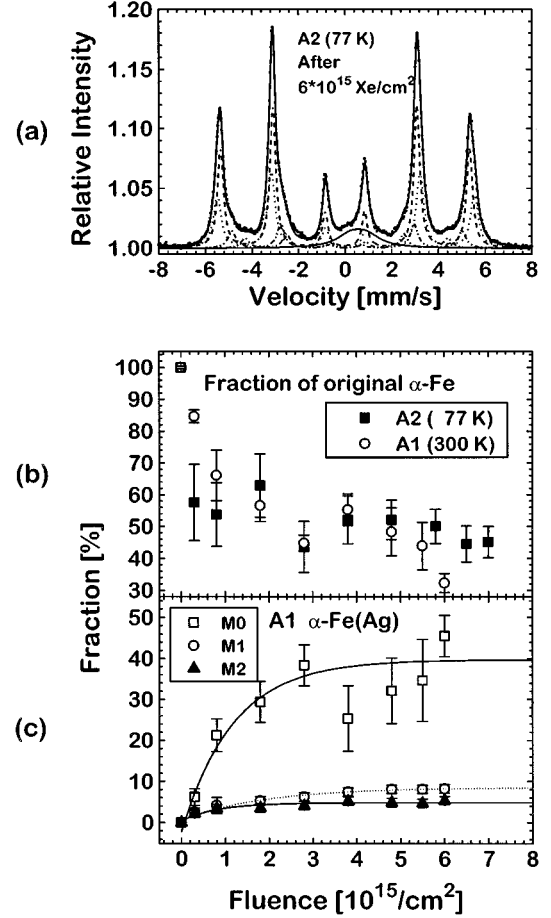


FIG. 13. (a) CEMS spectrum of a sample irradiated with 450 keV Xe⁺ ions at 77 K with $\Phi = 6 \times 10^{15}$ Xe/cm², (b) fraction of α -Fe as a function of the ion fluence for 450 keV Xe irradiation at 77 and 300 K, (c) fractions of the additional magnetic subspectra $M0$, $M1$, and $M2$ as a function of the ion fluence for 750 keV Xe ions at 300 K.

IV. DISCUSSION

Ion-beam mixing of metallic bilayers has been studied for a variety of systems and ions. The results have been reviewed, e.g., by Cheng,⁵ by Nastasi and Mayer,²⁴ and by Bolse.⁶ For most miscible systems (having a negative heat of mixing $\Delta H_{mix} < 0$), the mixing efficiency

$$\eta = \frac{\Delta\sigma_{mix}^2}{\Phi F_D}, \quad (6)$$

defined as the interface broadening $\Delta\sigma_{mix}^2$ per incident ion and deposited energy density F_D at the interface was found to be constant. This linear correlation between the mixing rate $k = \Delta\sigma_{mix}^2/\Phi$ and F_D points to either ballistic^{1,2} or local spike⁶ mixing. For large negative values of ΔH_{mix} , chemical driving of the irradiation-induced atomic transport was clearly demonstrated, e.g., for the systems Ni/Al,²⁵ Ni/Sb,²⁷ Sb/Al,^{27,28} and was attributed to diffusion in local thermal spikes. In addition, x-ray-diffraction, transmission electron microscopy (TEM) and hyperfine methods like perturbed an-

gular correlation (PAC) and CEMS have convincingly proven the formation of crystalline intermetallic compounds at the interface.^{6,25–30,22}

The situation in the thermally immiscible Fe/Ag system is different as the formation of compounds or alloys is forbidden in thermodynamical equilibrium. In a recent PAC and CEMS study of Xe-irradiated In/Fe and Ag/Fe bi- and multilayers, Neubauer and co-workers³¹ have identified several point defects associated with Ag atoms in the neighborhood of the hyperfine probes. However, these authors did not find any evidence of the formation of a binary crystalline or amorphous phase. According to an x-ray study of the ion mixing of Ag/Fe multilayers, Krebs *et al.*³² proposed that ballistic mixing in the collisional phase of the recoil cascade is counterbalanced by demixing and phase separation in the thermal spike phase. Although the formation of an atomic solution or a new phase would be suppressed by such balanced mechanisms, Ag-decorated defects may form as a consequence of long-range ballistic transport due to head-on primary collisions. These defects will then become visible in the PAC and Mössbauer spectra, even at low Ag concentrations.

The results obtained in the present work from RBS and STM analyses of Ag/Fe bilayers strongly support this interpretation. As mentioned above, the broadening obtained from RBS measurements $\Delta\sigma_{\text{RBS}}^2$ may contain two contributions: interface mixing and surface roughening. In most analyses of IBM experiments, it has been implicitly assumed that surface roughening and recrystallization of the top layer by the impinging ion beam is unimportant as compared to the strong interface mixing effect. However, in systems where a small or even vanishing mixing effect is expected, a quantitative separation of the two effects is necessary, as was shown by Sun *et al.*,³³ who investigated ion mixing of CrN_x-coated Al and found by utilizing STM that about 50% of the broadening observed in the RBS spectra was due to irradiation-induced surface roughening.

When comparing the quantities $\Delta\sigma_{\text{RBS}}^2$ (Figs. 6 and 7) and $\Delta\sigma_{\text{STM}}^2$ (Figs. 11 and 12) obtained for Ar- and Xe-irradiated Ag/Fe bilayers, it also turns out that the broadening observed with RBS is to a large extent determined by an increasing surface roughness. As discussed before, the difference $\Delta\sigma_{\text{RBS}}^2 - \Delta\sigma_{\text{STM}}^2$ can be regarded as a direct measure of the interface mixing effect and is plotted in Figs. 14 and 15 versus Φ . It is clear that the irradiation-induced atomic mixing at the interface is close to zero and, if present at all, much smaller than expected for ballistic processes. According to the model of Sigmund and Gras-Martí,^{1,2} ballistic mixing is given by the expression:

$$\Delta\sigma_{\text{bal}}^2 = (\Gamma_0/3\rho)(R_c^2/E_d)\Phi F_D, \quad (7)$$

where $\Gamma_0 = 0.608$ is a dimensionless constant, ρ is the average atomic density at the interface, E_d is the displacement threshold, and R_c is the minimum separation distance of a Frenkel pair. Taking $\rho = 7.166 \times 10^{22}$ atoms/cm³, $R_c = 1$ nm and $E_d = 20$ eV, we arrive at the ballistic interface broadening $\Delta\sigma_{\text{bal}}^2$ inserted as dashed lines in Figs. 14 and 15. It is evident that in all these cases the experimental values of $\Delta\sigma_{\text{mix}}^2 = \Delta\sigma_{\text{RBS}}^2 - \Delta\sigma_{\text{STM}}^2$ fall significantly below the calculated $\Delta\sigma_{\text{bal}}^2$ (see Table II). We therefore conclude that ballis-

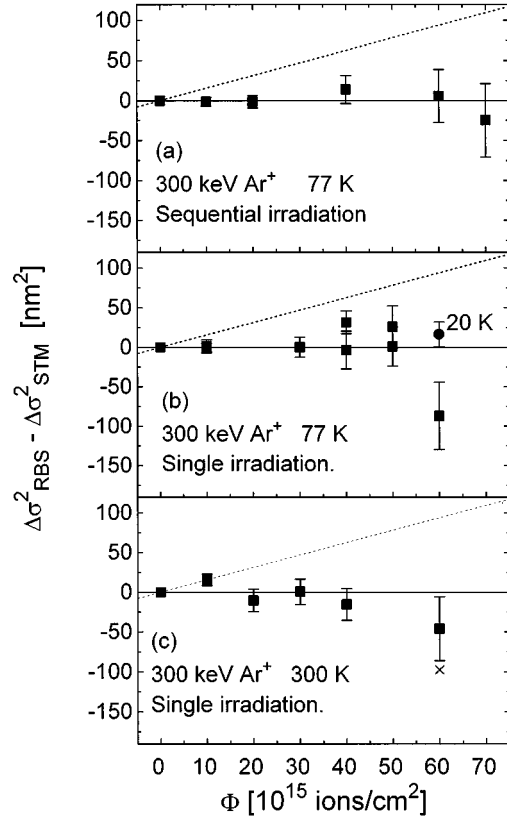


FIG. 14. Effective mixing $\Delta\sigma_{\text{mix}}^2 = \Delta\sigma_{\text{RBS}}^2 - \Delta\sigma_{\text{STM}}^2$ as a function of the ion fluence Φ : (a) for one single sample irradiated sequentially with 300 keV Ar at 77 K, (b) for a series of samples each of them irradiated in one step with 300 keV Ar ions at 77 K, and (c) for a series of samples each of them irradiated in one step with 300 keV Ar ions at 300 K.

tic mixing of the Ag/Fe interface, which should occur in any case, is to a large extent canceled by subsequent chemically driven relaxation processes.

It should be noted that in Figs. 14(b) and 14(c) the experimental points for the highest fluences fall below zero. We attribute this to the fact that in such cases, due to the high Ag sputtering yield, part of the Fe film might already be exposed to the surface, causing a perturbation to the STM measurements. In the particular case of 14(c), for instance, the height distribution of the corresponding sample does not appear as a Gaussian any more but exhibits a long tail at the left side of the distribution. The assumed linear additivity of $\Delta\sigma_{\text{mix}}^2$ and $\Delta\sigma_{\text{STM}}^2$ is therefore not strictly valid anymore. This is illustrated in Fig. 14(c), where the data point labeled by the symbol \times refers to $\Delta\sigma_{\text{STM}}^2$ as calculated from the asymmetric surface height distribution. When estimating $\Delta\sigma_{\text{STM}}^2$ from a Gaussian fitted to that fraction of the distribution which is not affected by the tail, a better agreement with the data obtained at lower fluences is achieved (full square with error bar).

According to the fractal approach to the collision cascades,⁵ Ag/Fe belongs to those materials ($\bar{Z} > 20$) where thermal spikes should be easily initiated and atomic transport should occur by transient diffusion in a liquidlike state. It would therefore be reasonable to argue that the ballistically intermixed Ag/Fe interface rearranges by subsequent spike-

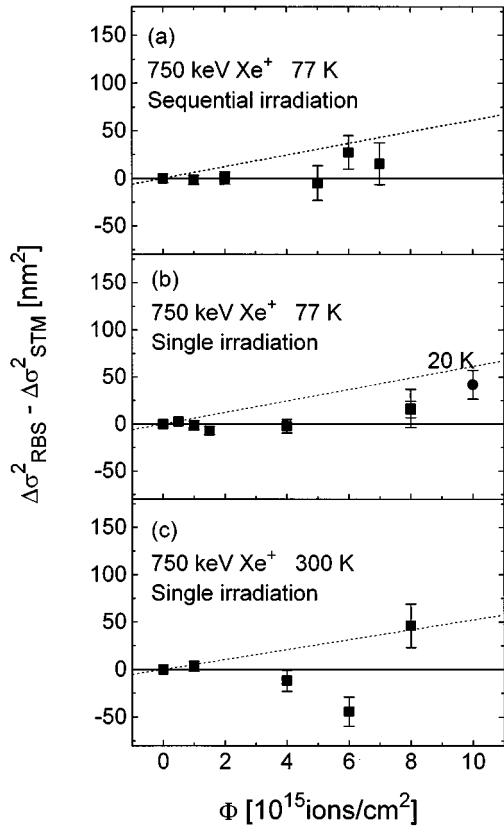


FIG. 15. Effective mixing $\Delta\sigma_{\text{mix}}^2 = \Delta\sigma_{\text{RBS}}^2 - \Delta\sigma_{\text{STM}}^2$ as a function of the ion fluence Φ : (a) for one single sample irradiated sequentially with 750 keV Xe at 77 K, (b) for a series of samples each of them irradiated in one step with 750 keV Xe ions at 77 K and 20 K (circle), and (c) for a series of samples each of them irradiated in one step with 750 keV Xe ions at 300 K.

induced demixing. This interpretation is supported by the results of ion mixing performed by Averback *et al.*⁸ on Cu/Nb, Cu/Bi, Cu/Mo and ⁶³Cu/⁶⁵Cu bilayer couples. These authors found that those systems which are miscible in the liquid, but not in the solid state, are intermixed by ion irradiation at 6 K but exhibit no mixing when irradiated at 300 K. The system Cu/Mo which is immiscible also in the liquid state does not mix at any temperature, as we have also ob-

TABLE II. Deposited energy density F_D at the Ag/Fe interface, ballistic mixing predicted by the model of Sigmund and Gras-Martí (Ref. 2), and the difference of the broadenings observed by RBS and STM as a function of the ion species and irradiation temperature.

		F_D^a (keV/nm)	$\Delta\sigma_{\text{bal}}^2/\Phi$ (nm ⁴)	$(\Delta\sigma_{\text{RBS}}^2 - \Delta\sigma_{\text{STM}}^2)/\Phi^b$ (nm ⁴)	
Ar	20 K	1.10	0.155	0.030	0.030
	77 K	1.10	0.155	0.016	0.019
	300 K	1.10	0.155	-0.024	0.028
Xe	20 K	4.60	0.645	0.420	0.100
	77 K	4.60	0.645	0.080	0.080
	300 K	3.90	0.550	-0.160	0.150

^aCalculated with TRIM.

^bWeighted fits from Figs. 14 and 15.

served for Ag/Fe. Such behavior would perfectly agree with a thermal spike scenario with small molten volumes across the interface, where interdiffusion or demixing (of the ballistically intermixed atoms) may take place, depending on whether the liquid phases are miscible or not. Thus, the completely immiscible bilayer couple remains unmixed, while quenching of the miscible liquids conserves the composition of the intermixed melt. At an irradiation temperature of 300 K also in those systems which do mix at low-temperature irradiation, intermixing is obviously counterbalanced by thermally activated demixing, most likely due to chemically guided radiation enhanced diffusion (RED). In contrast to such an interpretation, Kelly and Miotello³⁴ presented an ion-induced atomic transport mechanism without invoking any thermal spikes. According to their approach, chemical guidance of ion mixing originates from thermally activated residual defect motion at the ambient target temperature. However, our experiments performed at 20 K clearly exclude such a mechanism, since the target temperature was below annealing stage I_E (32 K for Ag, 120 K for Fe),³⁵ where long-range migration of interstitials and vacancies is suppressed. If residual defect motion were important, no demixing should occur at 20 K and the whole ballistic effect should be visible. Furthermore, the residual interstitials would become mobile during warming up of the sample to 300 K, which should result³⁴ in additional demixing and thus in different RBS spectra at 20 and 300 K. This was clearly not the case, and we therefore conclude that residual defect motion does not contribute to the ion induced atomic transport in the Ag-Fe system at low temperatures.

The above results are nicely supported by the CEMS experiments. If one assumes that a number of atoms equivalent to an Ag layer of about 0.2 nm dissolve uniformly in a 6.5 nm ⁵⁷Fe layer, one can reproduce the 2.4 at. % Ag concentration in α -Fe deduced from Mössbauer spectroscopy. From ballistic calculations, one would expect an equivalent of about 6 nm Ag to be dissolved in the Fe matrix. This means that only a very small net mixing remains at the interface, which is most probably caused by long-range relocations of Ag atoms (recoil implantation). Primary knock-on collisions may transport a small number of Ag atoms far into the α -Fe matrix, where they cannot participate in segregation and relaxation processes at the interface. These atoms will stay at their impurity sites where they are observed with the hyperfine methods (PAC and CEMS).^{22,31}

The atomic solution of about 2.5% Ag in Fe, deduced from Mössbauer spectroscopy, is higher than the solubility in thermodynamical equilibrium at 300 K (0.001 at. %),³⁶ but not as large as the values obtained after vapor quenching (up to 30 at. % Ag).³⁷ This means that the processes during ion irradiation are not as far from thermodynamical equilibrium as in vapor quenching. A similar conclusion was reached in the case of the immiscible system Fe/Mg.¹⁰ In agreement with the results of Neubauer *et al.* and Krebs *et al.*, and in contrast to Pan and Liu³⁸ we did not observe the formation of any secondary phase.

The increase of the surface roughness under ion bombardment is, to a large extent, determined by the increase of the size of the Ag grains and by their shape and orientation. Surface roughening due to sputter effects seems to be less important in the present case. After deposition of the Ag films the surface consists of half-sphere-shaped grains of

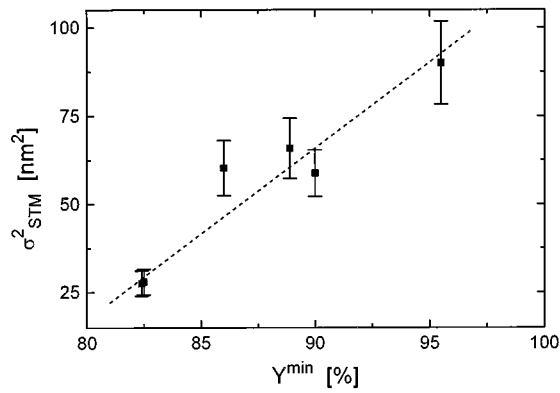


FIG. 16. Correlation between the variance σ_{STM}^2 of the surface height distribution and the minimum yield Y^{\min} of the Ag RBS subspectra.

about 30–50 nm in diameter, and the variance of the surface height distribution (σ_{STM}^2) is about 10 nm². As can be seen in Fig. 10, which shows the STM images of samples irradiated with 4×10^{16} Ar/cm², both low-temperature and room-temperature irradiation, cause strong recrystallization and grain growth. However, while the room-temperature irradiation seems to result in almost spherically shaped grains (150–300 nm in diameter) and an increase of σ_{STM}^2 by a factor of 10, irradiation at 77 K produces a much smoother surface of platelike structure with $\sigma_{\text{STM}}^2 \approx 50$ nm². The difference in the ion-induced recrystallization at low and room temperature can also be seen in the film texture after ion bombardment. Low-temperature irradiation results in a highly oriented film, as can be seen by the strong channeling effects shown in Fig. 9 for 20 and 77 K irradiations. Channeling measurements on a 300-K-irradiated sample reveal a much less textured surface. The relationship between the surface texture and the roughness becomes visible also in Fig. 16, which shows the roughness parameter σ_{STM}^2 plotted versus the observed minimum yield Y^{\min} in the channeling measurements. It turns out that the higher the orientation of the surface, the smaller is its roughness. Again, we take this as a hint that transient diffusion in thermal spikes is the most prominent transport mechanism at low temperature, while at room temperature also thermally activated defect migration becomes important. Local thermal spikes of some nm in diameter are formed *inside* the Ag film and recrystallization and grain growth should occur by fusing of grain boundaries and subsequent solidification. Since in the thin film grain boundaries are mainly perpendicular to the surface, grain growth by such a mechanism is expected preferentially in

lateral direction, as observed in the experiment. As soon as thermally activated long-range defect migration becomes possible (as for 300-K irradiation), grains may grow in three dimensions and become spherically shaped. This effect probably also explains the different roughnesses observed for the single and sequentially irradiated samples: Partial three-directional recrystallization might occur by defect recovery during warming up of the sample to 300 K between each irradiation step, which could (in addition to small irradiation direction variations) suppress texture formation in the sequentially irradiated samples much more than in the single irradiation mode. Our results agree well with the experiments presented by Hasegawa *et al.*,³⁹ who investigated grain growth by 2–3 keV Ar ions at room and at higher temperatures. However, contrary to their interpretation which attributes the grain growth to a thermally activated process by beam heating of the sample during irradiation, the different structure of the grains obtained by low-temperature irradiation suggests that the mechanism most likely involves diffusion *inside* the thermal spikes, as described above and also suggested by other authors.^{40,41}

In conclusion, we have shown that ballistic ion mixing of the Ag/Fe interface is significantly counterbalanced by a chemically driven relaxation mechanism, which results in demixing of the two materials and which is most probably a thermal spike diffusion process. Nevertheless, the small Ag concentration achieved in Fe is still much higher than in thermodynamical equilibrium. According to the observed temperature dependence of the effects, transient diffusion in local thermal spikes seems to be the most likely demixing mechanism, while the supersaturation is attributed to long-range recoil implantation. This interpretation is supported by the ion-induced recrystallization behavior and the observed correlation between the surface texture and the roughness. The grain shape observed at a low irradiation temperature is attributed to a thermal-spike-induced grain growth process, while additional thermally activated diffusion is needed to explain the surface structure after room-temperature irradiation.

ACKNOWLEDGMENTS

The authors are grateful to D. Purschke for expertly running the IONAS accelerator, to Dr. M. Uhrmacher, Dr. H. U. Krebs, and M. Neubauer for illuminating discussions and to Professor G. von Minnigerode for his interest in the STM analyses. One of the authors (A.C.S.) is also indebted to DGAPA-UNAM, Mexico, for financial support during his Ph.D. studies in Göttingen. This work was funded by the Deutsche Forschungsgemeinschaft (DFG).

¹P. Sigmund and A. Gras-Martí, Nucl. Instrum. Methods **168**, 389 (1980).

²P. Sigmund and A. Gras-Martí, Nucl. Instrum. Methods **182/183**, 25 (1981).

³T. W. Workman, Y. T. Cheng, W. L. Johnson, and M. A. Nicolet, Appl. Phys. Lett. **50**, 1485 (1987).

⁴W. L. Johnson, Y. T. Cheng, M. V. Rossum, and M. A. Nicolet, Nucl. Instrum. Methods Phys. Res. Sect. B **7/8**, 657 (1985).

⁵Y.-T. Cheng, Mater. Sci. Rep. **5**, 45 (1990).

⁶W. Bolse, Mater. Sci. Eng. R **12**, 53 (1994).

⁷A. Miotello and R. Kelly, Surf. Sci. **314**, 275 (1994).

⁸R. S. Averback, D. Peak, and L. J. Thompson, Appl. Phys. A **39**, 59 (1986).

⁹A. Gupta, G. Principi, P. Trotta, E. Jannitti, C. Tosello, L.M. Gratton, S. Enzo, S. Lo Russo, and V. Rigato, Surf. Coat. Tech. **51**, 429 (1992).

- ¹⁰C. Jaouen, J. Delafond, N. Junka, and P. Goudeau, Nucl. Instrum. Methods Phys. Res. Sect. B **43**, 34 (1989).
- ¹¹D. Marton, J. Fine, and G. P. Chambers, Phys. Rev. Lett. **61**, 2697 (1988).
- ¹²B. Y. Tsaun and J. W. Mayer, Appl. Phys. Lett. **37**, 4 (1980).
- ¹³F. R. de Boer, R. Boom, W. C. M. Mattens, A. R. Midema, and A. K. Niessen, *Cohesion in Metals* (North-Holland, Amsterdam, 1988).
- ¹⁴M. Uhrmacher, K. Pampus, F. J. Bergmeister, D. Purschke, and K. P. Lieb, Nucl. Instrum. Methods Phys. Res. Sect. B **9**, 234 (1985).
- ¹⁵J. P. Biersack and L. G. Haggmark, Nucl. Instrum. Methods Phys. Res. Sect. B **174**, 257 (1980).
- ¹⁶L. R. Doolittle, Nucl. Instrum. Methods Phys. Res. Sect. B **9**, 344 (1985).
- ¹⁷L. R. Doolittle, Nucl. Instrum. Methods Phys. Res. Sect. B **15**, 227 (1986).
- ¹⁸P. Schaaf, A. Krämer, L. Blaes, G. Wagner, F. Aubertin, and U. Gonser, Nucl. Instrum. Methods Phys. Res. Sect. B **53**, 184 (1991).
- ¹⁹W. Kündig, Nucl. Instrum. Methods Phys. Res. Sect. B **75**, 336 (1969).
- ²⁰F. E. Wagner, J. Phys. (Paris) Colloq. **37**, C6-673 (1976).
- ²¹U. Gonser and P. Schaaf, Fresenius Z. Anal. Chem. **341**, 131 (1991).
- ²²M. Neubauer, K. P. Lieb, P. Schaaf, and M. Uhrmacher, Thin Solid Films **275**, 69 (1996).
- ²³P. Schaaf, A. Crespo-Sosa, K. P. Lieb, W. Bolse, and C. Tosello, in *Proceedings of the International Conference on the Application of the Mössbauer Effect (ICAME '95)*, Rimini, Italy, 1995, edited by I. Ortalli and R. Barbini, Conf. Proc. SIF (Editrice Compositori Bologna, Bologna, 1996), Vol. 50, p. 695.
- ²⁴M. Nastasi and J. W. Mayer, Mater. Sci. Eng. R **12**, 1 (1994).
- ²⁵T. Weber and K. P. Lieb, J. Appl. Phys. **73**, 3499 (1993).
- ²⁶F. Shi, T. Weber, W. Bolse, and K. P. Lieb, Appl. Phys. A **57**, 343 (1993).
- ²⁷F. Shi, W. Bolse, K. P. Lieb, and J. P. Wilbrandt, Nucl. Instrum. Methods Phys. Res. Sect. B **89**, 382 (1994).
- ²⁸F. Shi, W. Bolse, and K. P. Lieb, J. Appl. Phys. **78**, 2303 (1995).
- ²⁹K. P. Lieb, W. Bolse, and M. Uhrmacher, Nucl. Instrum. Methods Phys. Res. Sect. B **89**, 277 (1994).
- ³⁰M. Uhrmacher, P. Wodniecki, F. Shi, T. Weber, and K. P. Lieb, Appl. Phys. A **57**, 353 (1993).
- ³¹M. Neubauer, K. P. Lieb, P. Schaaf, and M. Uhrmacher, Phys. Rev. B **53**, 10 237 (1996).
- ³²H. U. Krebs, Y. Luo, M. Störmer, A. Crespo, P. Schaaf, and W. Bolse, Appl. Phys. A **61** 591 (1995).
- ³³J. Sun, W. Bolse, K. P. Lieb, and A. Traverse, Mater. Sci. Eng. A **229**, 196 (1995).
- ³⁴R. Kelly and A. Miotello, Nucl. Instrum. Methods B **59/60**, 515 (1991).
- ³⁵*Vacancies and Interstitials in Metals*, edited by A. Seeger, D. Schumacher, W. Schilling, and J. Diehl (North-Holland, Amsterdam, 1970).
- ³⁶*Binary Alloy Phase Diagrams*, edited by T. B. Massalski (American Society for Metals, Metals Park, OH, 1986).
- ³⁷K. Sumiyama, Vacuum **41**, 1211 (1990).
- ³⁸F. Pan and B. X. Liu, J. Phys. Condens. Mater. **5**, L315 (1993).
- ³⁹Y. Hasegawa, Y. Fujimoto, and F. Okuyama, Surf. Sci. **163**, L781 (1985).
- ⁴⁰J. C. Liu and J. W. Mayer, Nucl. Instrum. Methods Phys. Res. Sect. B **19/20**, 538 (1987).
- ⁴¹D. E. Alexander and G. S. Was, Phys. Rev. B **47**, 2983 (1993).